Analysis of the Magnetic Field for the ZEUS Luminosity Spectrometer

Monica Skoge

August 2001

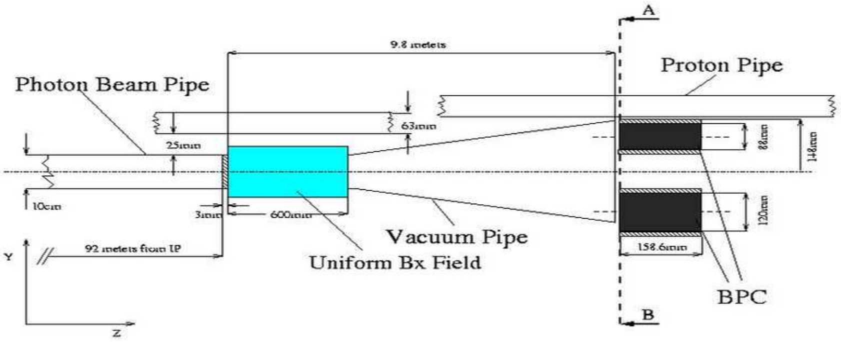

Figure 1: *The design setup for the luminosity spectrometer*

1 The New ZEUS Luminosity Spectrometer

Since 1992 HERA, an electron-proton collider located at DESY in Hamburg, Germany, has been testing our understanding of the strong force and the predictions of quantum chromodynamics. A luminosity upgrade is currently underway at HERA, which is expected to bring integrated luminosities of $1fb^-1$ by 2005. A common way to measure the luminosity is to count the number of photons produced in the well-understood Bethe-Heitler process ($ep \to ep\gamma$), in which an electron passing close to a proton is accelerated by its potential and radiates a photon. In preparation for the future high luminosity operation at HERA, a new luminosity spectrometer has been designed to circumvent the problems expected by a more intense photon beam.

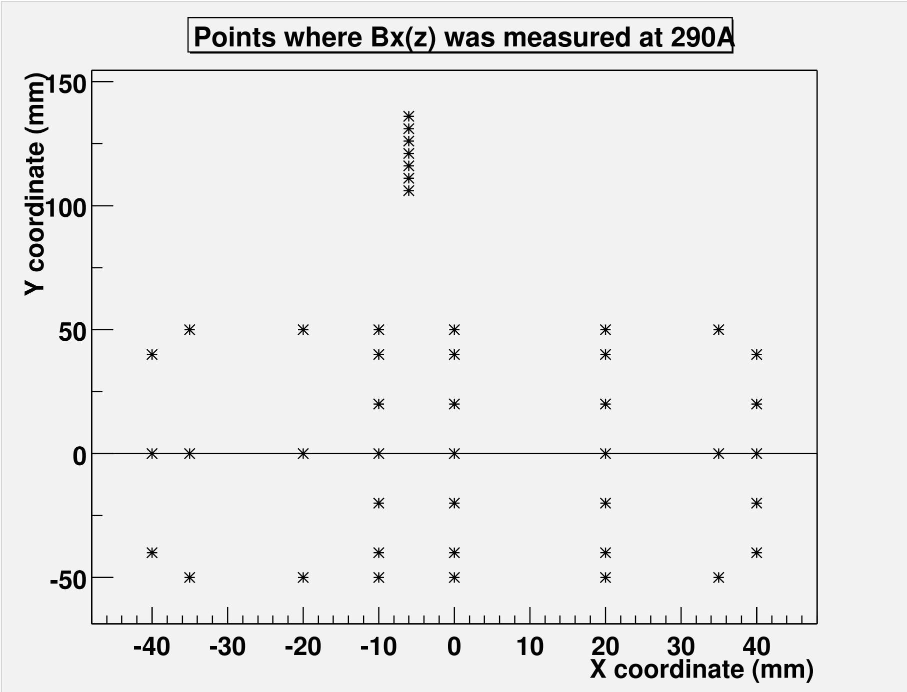

Figure 2: *The points at which the Bx component of the magnetic field was measured*

These problems include primary synchroton radiation damage to the calorimeter and multiple event pile-ups. In the new design, photons produced in the Bethe-Heitler process pass through an exit window located 92 meters downstream from the interaction point and are converted into electron-positron pairs, which are then separated by a dipole magnet and detected in two calorimeters, positioned above and below the radiation beam as shown in Fig. 1. This design naturally avoids placing the calorimeters directly in the radiation beam and limits multiple event pile-ups because only 10 percent of the photons convert in the exit window into electron/positron pairs and the overall acceptance is of the order of 3 percent.
The luminosity is calculated by dividing the rate of events in the calorimeters by the product of the acceptance and the cross-section for the Bethe-Heitler process. Good calorimeter resolution and understanding of the theoretical cross-section for the Bethe-Heitler process in the energy range used by the spectrometer enable the total systematic error in the luminosity to be 1 percent, provided that the uncertainty in the acceptance be calculated to within 1 percent. An accurate knowledge of the acceptance is key to an accurate measurement of the luminosity. Three main factors affect the acceptance: the conversion rate in the exit window, particle deflection due to the magnetic field, and the geometry of the calorimeters. Using measurements

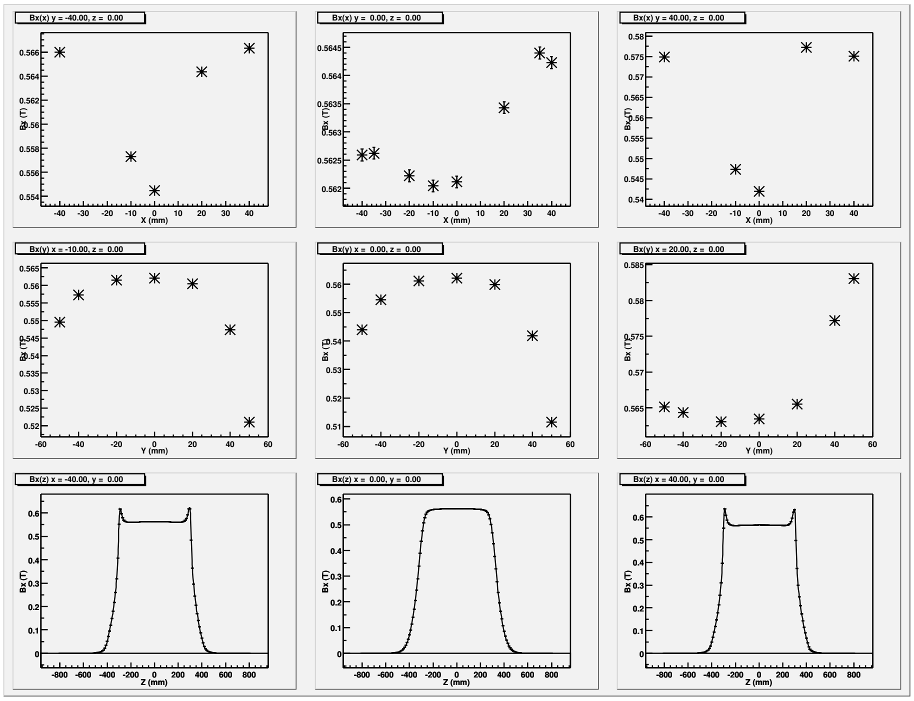

Figure 3: *Measured Bx values plotted as functions of x, y, and z*

of the B_x component of the magnetic field at various points, I constructed a magnetic field map and studied the deflection of particles from the field with the ultimate goal of determining how the uncertainty in the magnetic field affects the uncertainty in the overall acceptance.

2 Analysis of the B_x component

The Zeus luminosity spectrometer is using a 60 cm long dipole magnet with a 10 cm bore and nominal field strength of 0.5 Tesla. The error in the measurement is $0.0001 * measuredvalue + 0.00006 * 0.8$ or approximately 0.01 percent. In my analysis I used the convention that the positive z-direction points downstream from the interaction point in the direction of the incoming photons and the positive y-direction points up.
I began my analysis of the magnetic field with only the B_x component measured every 10 mm in the z-direction and at the various x and y values shown in Fig. 2. All the B_x values at $x \geq -10mm$ were negative, whereas the rest were positive and this was attributed to the measurer having flipped the instrument. To get an idea of the shape of the magnetic field,

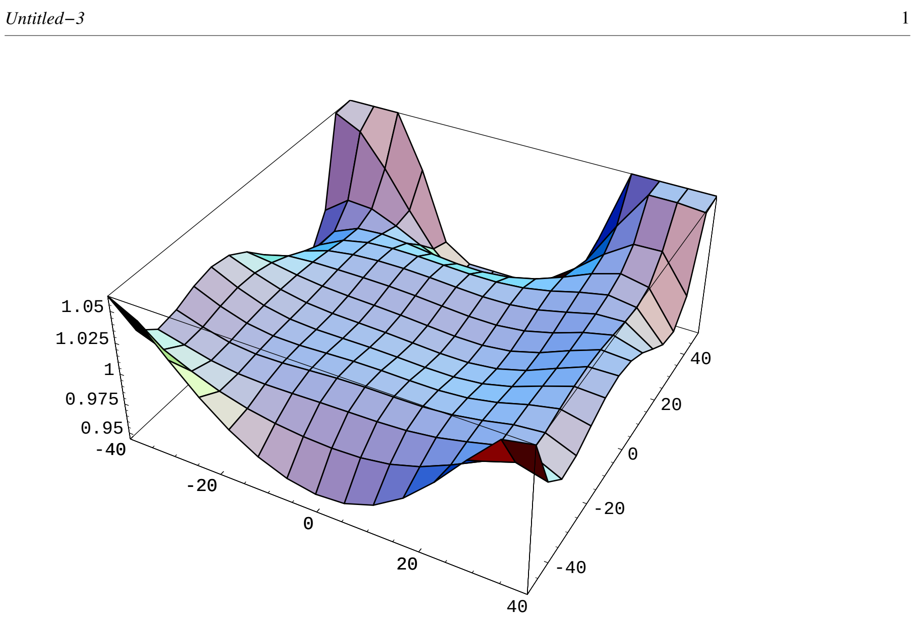

Figure 4: *Integral Bxdz as a function of x(mm) and y(mm) linearly fit with* $R^2 = 0.9806$ *normalized at the point (0, 0)*

I graphed B_x(x), B_x(y), and B_x(y) for different values of fixed x, y, and z and obtained the graphs of Fig. 3. B_x(y) seems to have a smooth parabolic shape, which switches concavity as $|y|$ increases. B_x(x) seems to jump around more, but generally increases as $|x|$ increases and B_x(z) has a well-defined plateau shape with small overlayed gaussian peaks at z=-300 and 300 mm, that show up only at x=40 and -40 mm. A midpoint approximation was used to calculate the $\int B_x dz$ for all the measured points. Fig. 4 shows a normalized 3D plot of the $\int B_x dz$ and Fig. 5 shows representative cross-sections. The $\int B_x dz$ varies by approximately 5 percent.

3 Calculating the B_y and B_z components

3.1 Symmetry arguments and boundary conditions

The B_y and B_z components of the field were calculated using Maxwell's equations. From the z-component of the curl of the B-field, we know that

$$B_y(x, y, z) = \int_0^x \frac{\delta B_x(x', y, z)}{\delta y} dx' + B_y(0, y, z) \tag{1}$$

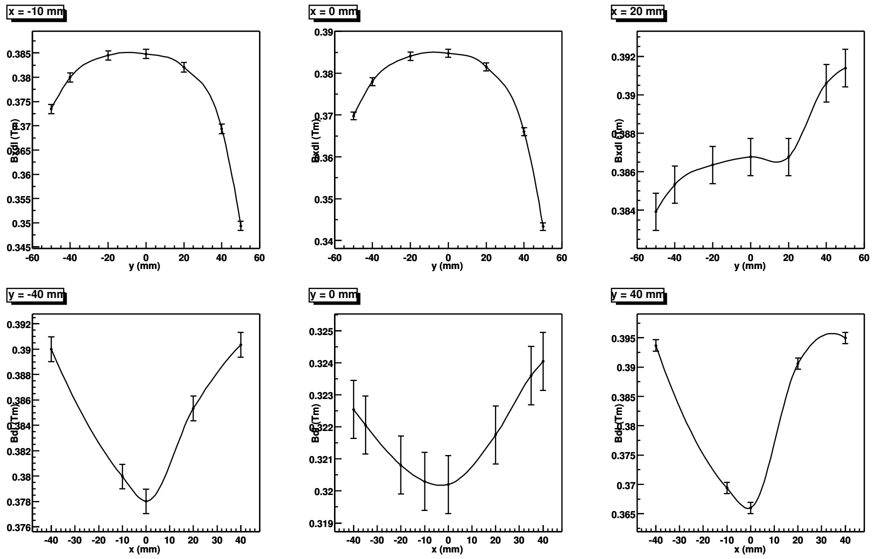

Figure 5: *Integral Bxdz as a function of x and y*

Using the assumption that the field is symmetric with respect to the y-z plane at x = 0, from the divergence equation it follows that

$$\frac{\delta B_y(0,y,z)}{\delta y} = -\frac{\delta B_z(0,y,z)}{\delta z} \tag{2}$$

A solution to the above equation is By(0,y,z) = Bz(0,y,z) = 0. It can be proven from Maxwell's equations that the solution is unique. Another way of obtaining the same result is to assume that the y-z plane is a plane of symmetry about x = 0 and the x-y plane is a plane of symmetry about z = 0. From symmetry arguments, it follows that By(0,y,z) = Bz(0,y,z) = 0. In the real magnet however, the proton pipe, which runs parallel to the z-direction just above the magnet, breaks the assumed symmetries. The proton pipe is off-centered by 8 mm in the x-direction, which significantly breaks the y-z plane of symmetry as can be seen in the upper plots of Fig. 3. To get a measure of the significance of the asymmetry in x, $\frac{\delta B_x}{\delta x}$ was calculated at x = 0 by fitting the measured points with a second or fourth order polynomial depending on the number of available points and taking the derivative. The resulting values for $\frac{\delta B_x}{\delta x}$ at x = 0 are shown in Fig. 11. The mean value is $7*10^{-}5$ and the values are highest at the fringe regions where z = -300 and 300 and y = 50. Thus in the center of the magnet the field can be roughly approximated as symmetrical with respect to the y-z axis at x = 0. The proton pipe also rises slightly upward in the positive z-direction and breaks the x-y plane of symmetry. This is a very

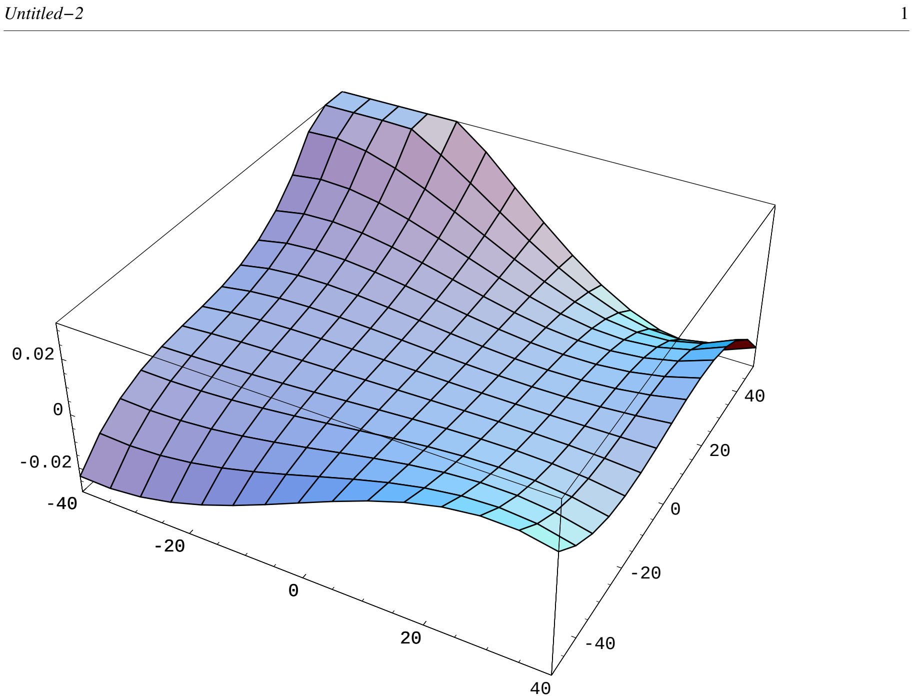

Figure 6: *Integral Bydz as a function of x and y linearly fit with* $R^2 = 0.9906$ *calculated from the By components of the field*

small effect and can barely be noticed in the bottom graphs of Fig. 3.

3.2 Algorithm for calculating the B_y component

For the B_y component at a point (x', y', z'), I fit $B_x(y)$ at x = x' - δx and x = x', took the derivatives at y', averaged them, and then multiplied the average by δx to get the change in B_y. My boundary assumptions as discussed in the previous section were that $B_y = 0$ on the y-z plane going through the center of the magnet where x = 0. I thus had to start from the center of the magnet and proceed outward moving a distance δx and adding the calculated change in B_y to the current value of B_y. However, I could not find a function that fit B_x(y) well. I had from 3-7 points to work with, which limited me to low order polynomials. The chisquared values for the second degree fit were of the order of 1000 and those of the fourth degree fit were of the order of 100.

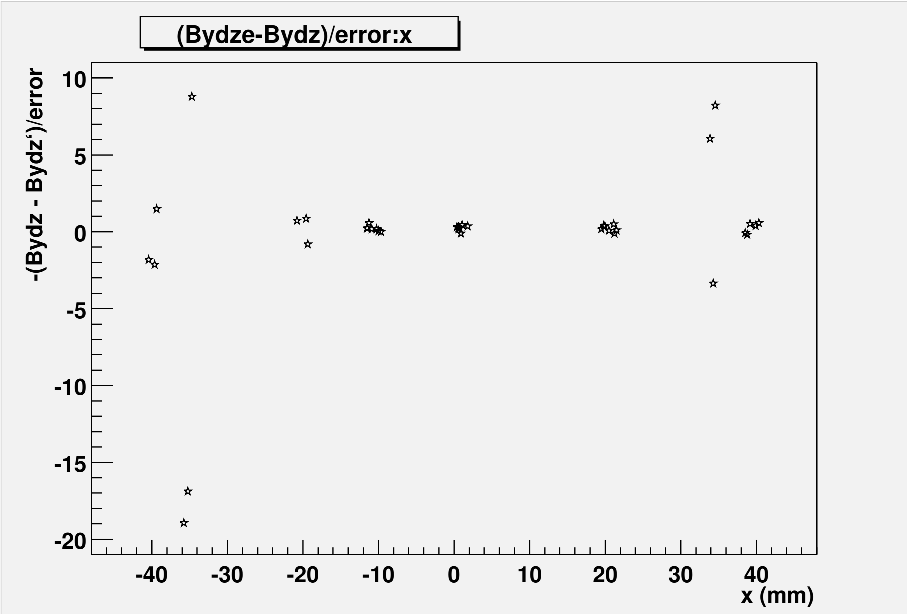

Figure 7: *Comparison of Integral Bydz calculated by 2 different methods*

3.3 Calculation of

$$\int B_y dz$$

I used the calculated B_y values to find the $\int B_y dz$, which is plotted in Fig. 6. I also found the $\int B_y dz$ directly from the $\int B_x dz$ with the same procedure as before, except that the B_x values were replaced with the $\int B_x dz$. I was able to get a rough estimate of the error by propagating the parameter errors from the polynomial fits. A comparison of the $\int B_y dz$ values obtained from the two methods, which interchanged the order of calculating the B_y components and integration is shown in Fig. 7. They agree fairly well in the center of the magnet, but disagree significantly at some high $|x|$ values. The mean $\int B_y dz$ is a half percent of the mean

$$\int B_x dz$$

.

3.4 The B_z component

I calculated the B_z components using the same procedure as for B_y. In this case, however, I had 160 points to work with in fitting B_x(z) and was able to come up with a decent fit. I

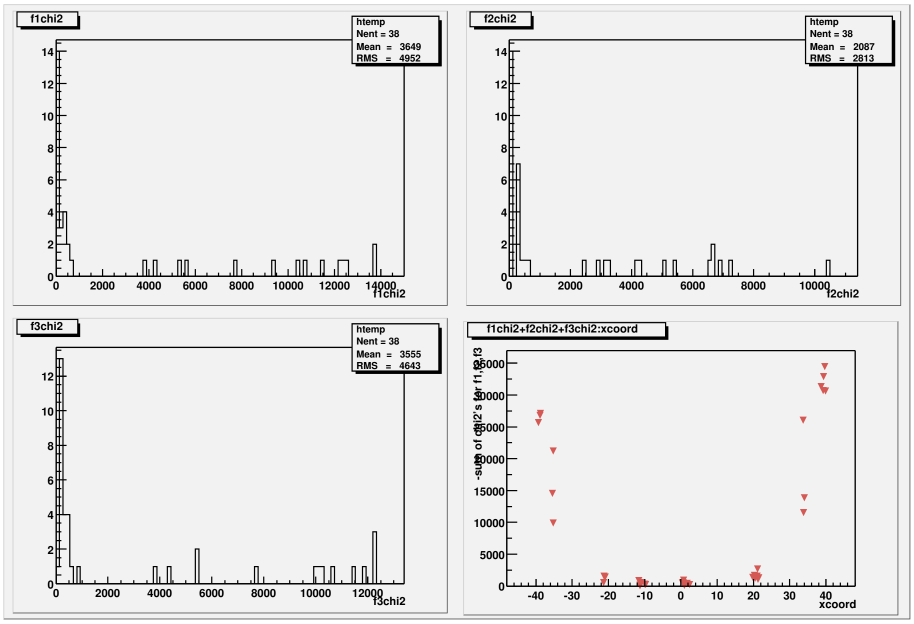

Figure 8: *Sum of the chi2 values for fits of f1, f2, and f3 versus x where f1 is a gaussian fit of Bx(z) from (-800–300mm), f2 is an 8th degree polynomial fit of Bx(z) from (-300-300mm) and f3 is a gaussian fit of Bx(z) from (300-800mm)*

divided the graph of B_x(z) into three sections: (-800 - -300 mm), (-300 - 300 mm), and (300 - 800 mm). The chisquares for the fits are shown in Fig. 8. The chisquares increase dramatically around x = 40 and -40, where there were small peaks at z = 300 and -300 on the graph of B_x(z), but are comparatively smaller in the central region. The $\int B_z dz$ is graphed in Fig. 9. The mean $\int B_z dz$ is only 0.02 percent of the mean $\int B_x dz$.

4 Particle Deflection

Using my approximated values for the $\int B_x dz$ and the $\int B_y dz$, I was able to approximate the deflection of the particles due to the B_x and B_y components of the field with the formula

$$d = \frac{0.3 * \int Bdz * dis}{p} \tag{3}$$

where d = the deflection in x or y, $\int Bdz = \int Bxdz$ or $\int Bydz$ in Tm, dis = the distance from the center of the magnet to the calorimeters, and p is the particle's momentum in GeV. My assumption in this model is that the particle is accelerated by the magnetic field in a circle and that

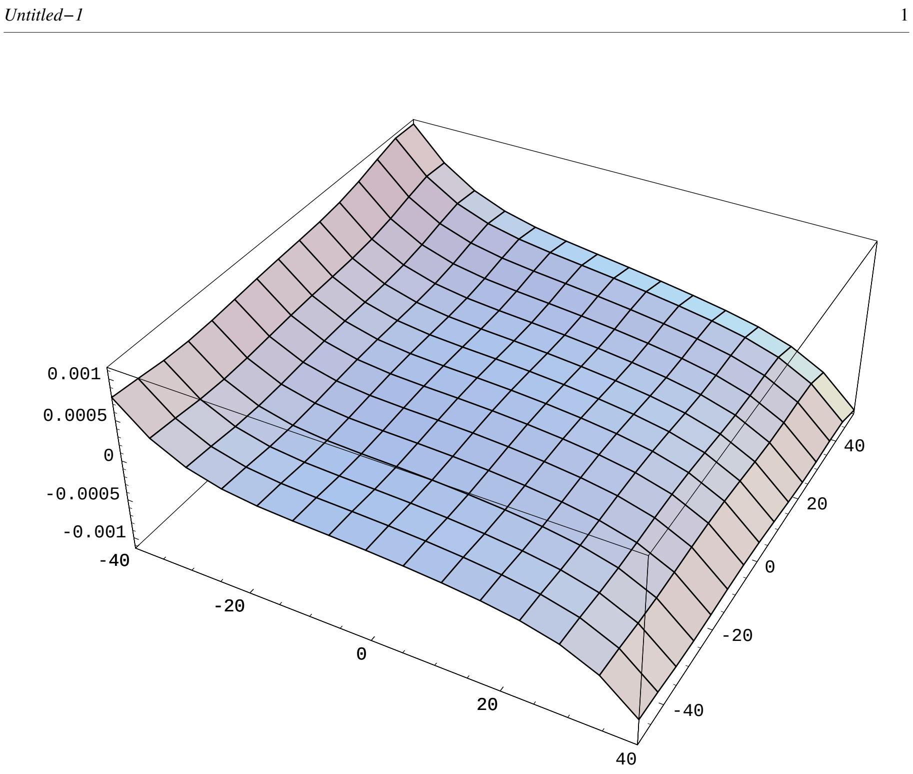

Figure 9: *Integral Bzdz as a function of* x *and* y *linearly fit with* $R^2 = 0.9901$

the particle's momentum perpendicular to the radius of the circle is constant. For deflections due to B_y and B_x, this momentum is the particle's longitudinal momentum of approximately 10GeV and is approximately constant. This model however does not work for deflections due to B_z because the B_z component is sensitive only to the particle's transverse momentum, not its longitudinal momentum, and this momentum is not constant. The transverse momentum is initially zero and increases slightly due to the Bx and By components. The particle's transverse momentum is so small and $\int B_z dz$ is such a small fraction of the $\int B_x dz$ that we can ignore the deflection due to B_z. Fig. 10 shows a plot of the deflection in the y-direction versus the $\int B_x dz$ and the deflection in the x-direction versus the $\int B_y dz$. Particles may be deflected in the x-direction by approximately 5 mm.

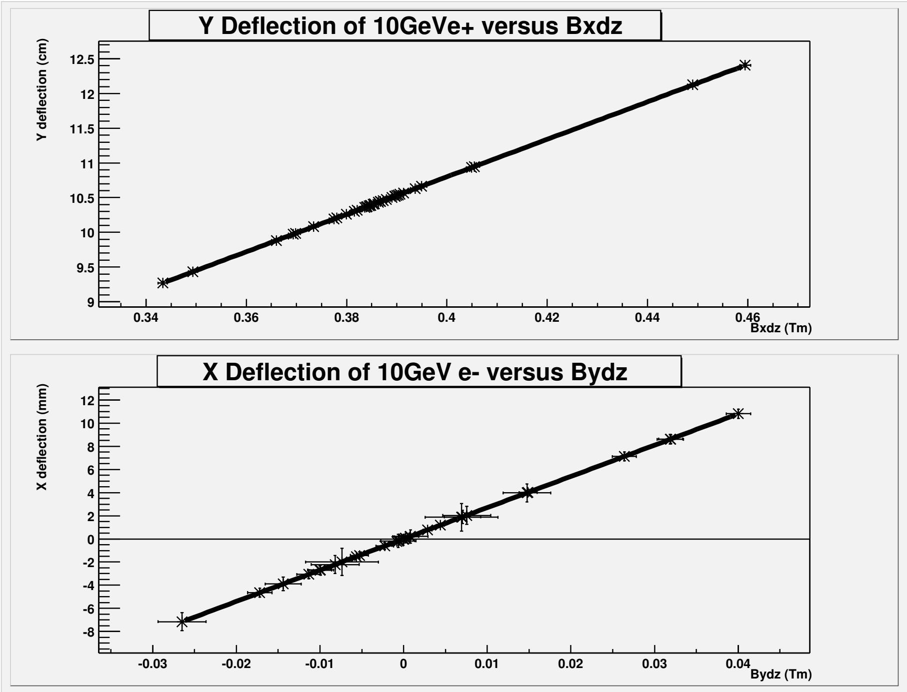

Figure 10: *Deflection of e+/e- in the magnetic field using the approximated formula: d = 0.3*Bdl*dis/p where d = the deflection in x or y, Bdl = the integral Bdl in Tm, dis = the distance from the center of the magnetic field to the calorimeter, and p is the particle's momentum in GeV*

5 Monte Carlo simulation of particle deflections and computer modelling

To get a better idea of particle deflections, the B_x components of the magnetic field were inputted into Geant, which has a more sophisticated particle deflection algorithm. The program which inputs the B_x components can also easily incorporate the B_y and B_z components. The interpolation was not done in Geant, but rather Geant makes bins and requires the values of each bin to be inputted. I had Geant make bins of size 1cm^3. The bins were created and the values of the bins were inputted so that the measured values corresponded to the center of the bins. Where measurements were lacking, I used my own methods of interpolation. My program that produces the input for Geant initially looks to see if there is a measurement at the desired point. If not, it next looks to see if there are enough measurements so that B_x can be fit as a function of x. If so, it evaluates the function at the desired x coordinate to get B_x. If there

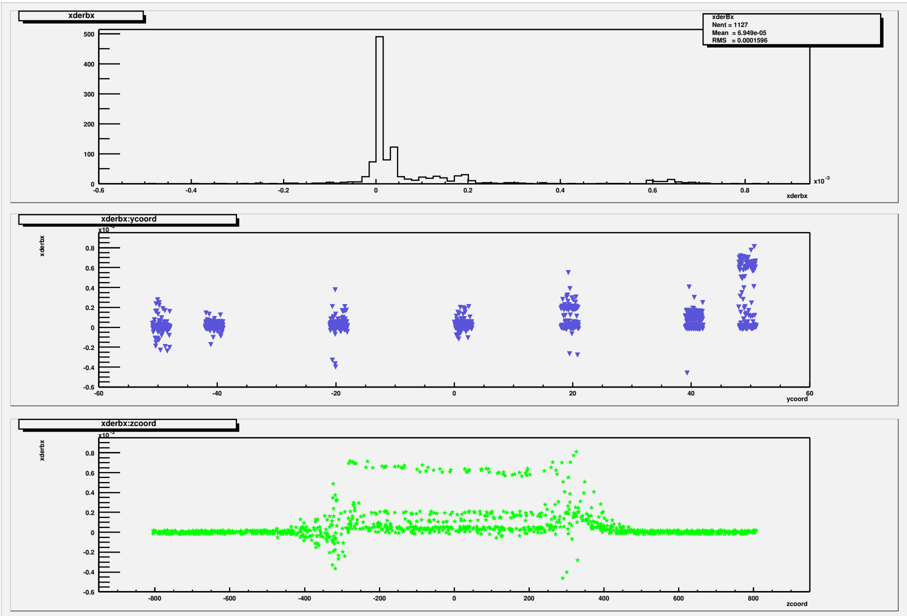

Figure 11: *Divergence of B field at (-10, 0, z)*

are not enough points, it then tries fitting in the y direction. If there are not enough points in the y-direction, the next option is to take an average of the values at the corners of the bin to get B_x. Finally, if all else fails, it fits B_x(x) above and below the desired point, evaluates the functions at the desired x coordinate, and takes the average. The geometry of the magnetic field and calorimeters is currently installed in Geant. Once the B_y and B_z components are inputted, we can begin to see how changing the magnetic field affects the acceptance.
A major difficulty thus far has been finding a decent fit to B_x(x) and B_x(y). Most recently I have been working with Opera, which is a program that calculates the magnetic field from the geometry and material properties of the magnet. The next step is to input the precise geometry of the magnet and proton pipe and compare the B field values calculated by Opera with the measured values. Because of the asymmetry of the magnet, Opera appears to be the most promising option in terms of calculating the B_y and B_z components of the field.

6 Conclusion

My role has been to set up the machinery for the next level of approximations of the magnetic field. Since the field is not symmetric with respect to the y-x plane about x = 0, a new method must be used to calculate the B_y and B_z components to a reasonable degree of precision. This new method will most likely be an iterative method and involve computer modelling and simulations. From my analysis I have found that the B_z component of the magnetic field appears to be negligible, whereas the B_y component is significant and may deflect the particles of the order of 5 mm. It is critical to find a better function for interpolating the data in order to obtain the desired uncertainty in the magnetic field of 2 percent.